Int J Mech Mater Des (2024) 20:233–249
https://doi.org/10.1007/s10999-023-09673-6

Hyperelastic constitutive model parameters identification using optical-based techniques and hybrid optimisation

Saeed Mollaee · David M. Budgett · Andrew J. Taberner · Poul M. F. Nielsen

Received: 26 December 2022 / Accepted: 12 August 2023 / Published online: 9 September 2023

Abstract In this paper we propose a new optical-based technique to identify the constitutive relation coefficients of the hyperelastic material using a hybrid optimisation approach. This technique can be used in place of traditional mechanical testing of elastomers for applications that involve inhomogeneous deformation. The purpose of the proposed method is to identify the incompressible hyperelastic material constitutive relation coefficients using a single experiment under different loading cases. The method comprises sample surface 3D reconstruction and uses finite element simulations to replicate the experiments, and uses a hybrid optimisation technique to minimise the error between actual 3D deformations and FE simulation results. The proposed hybrid technique predicts the hyperelastic constitutive relation coefficients more accurately than other optimisation methods. This study introduces a novel approach by employing a subpixel image registration algorithm for 3D reconstruction. The method requires a single experiment with diverse loading cases to accurately determine the coefficients of hyperelastic constitutive relations. The setup is portable and can be accommodated in a small suitcase. For this purpose, an apparatus was constructed comprising a stereoscopic system with eight cameras and a six-degree-of-freedom force-torque sensor to measure the induced forces and torques during the experiments. We identified the constitutive relation coefficients of Ogden N1, Ogden N3, Yeoh, and Arruda-Boyce relations which are commonly used models for silicone materials, using a traditional uniaxial test, optical uniaxial test (experiments performed using a constructed optical system), and inhomogeneous deformations tests. The study demonstrated that the coefficients obtained from inhomogeneous deformation tests provided the most accurate FE predictions. It was also shown that hyperelastic constitutive relation coefficients obtained from traditional uniaxial tests are insufficient to describe the material behaviour when the material undergoes inhomogeneous deformations.

Keywords Hyperelastic material · Uniaxial test · Inhomogeneous deformations · Optimisation · Hessian Matrix

S. Mollaee (✉) · D. M. Budgett · A. J. Taberner · P. M. F. Nielsen
Auckland Bioengineering Institute, The University of Auckland, 70 Symonds Street, Auckland, New Zealand
e-mail: smol775@aucklanduni.ac.nz

D. M. Budgett
e-mail: d.budgett@auckland.ac.nz

A. J. Taberner
e-mail: a.taberner@auckland.ac.nz

P. M. F. Nielsen
e-mail: p.nielsen@auckland.ac.nz

A. J. Taberner · P. M. F. Nielsen
Department of Engineering Science and Biomedical Engineering, The University of Auckland, 70 Symonds Street, Auckland, New Zealand

1 Introduction

Elastomers and rubber-like materials are widely used because of their unique properties such as low stiffness, high toughness, and high maximum strain (Amin et al. 2006; He et al. 2021). These make these materials suitable for a wide range of industrial and engineering requirements, such as conveyor belts, tyres, and biomedical applications (Sareh et al. 2014; Lee et al. 2017; Payne et al. 2015). In these applications the elastomer may undergo a variety of deformations, and thus it is critical to be able to predict the behaviour of the material under a wide range of stress–strain conditions.

Rubber-like materials can undergo large non-linear deformations (Dobrynin and Carrillo 2010). However, experimental measurements of the stress–strain relation for rubber-like materials reveal that the linear theory of elasticity does not capture the nonlinear mechanical properties of the material (Martins et al. 2006). Hyperelastic constitutive relations were formulated to address this issue and describe the mechanical behaviour of rubber materials assuming that the material does not have energy loss during deformation and does not exhibit viscous properties (Boyce and Arruda 2000; Steinmann et al. 2012; Zhao et al. 2019). There are two main categories of hyperelastic constitutive relations: phenomenological models, such as those developed by Yeoh and Ogden; and micromechanical network models like those of Arruda-Boyce (He et al. 2021).

It is common to select appropriate hyperelastic constitutive model parameters by comparing model predictions to corresponding experimental data (Madireddy et al. 2015; Bergström 2015). But since such materials often undergo large deformations, and the stress–strain behaviour varies significantly among materials, it is challenging to define a single form of strain-energy density function that adequately represents the stress–strain relation from any experiment (Kim et al. 2012). Elsayed et al. examined a reduced *N*-order polynomial and Ogden hyperelastic relation for Ecoflex 0030 and Ecoflex 00-50 and reported that, among the *N*-order polynomial relations considered, Ogden N3 was most suitable for Ecoflex 00-50 (Elsayed et al. 2014). Zhang et al. also used Ogden N3 for defining the stress–strain relation for Ecoflex 00-50 (Zhang et al. 2021). Sarkar et al. conducted a study involving the bending of a soft actuator and proposed that Yeoh is a suitable constitutive relation for the modelling of Ecoflex 00-50 (Sarkar et al. 2019). Shivapooja et al. designed a study and modelled the dynamic surface deformation of silicone elastomer with Ecoflex 0010 and Ecoflex 00-50, and suggested that the Arruda-Boyce formulation is a suitable hyperelastic relation for both (Shivapooja et al. 2015). Sparks et al. employed a first-order Ogden model (Ogden N1) to characterise the behaviour of Ecoflex 00-50 (Sparks et al. 2015). There thus remains a lack of consensus on the best hyperelastic constitutive model for defining the mechanical behaviour of a hyperelastic material (He et al. 2021; Dal et al. 2021; Külcü 2019; Bustamante and Rajagopal 2252; Anssari-Benam 2021).

Moreover, it is common to identify the model parameters based solely upon simple uniaxial stretch experiments (Martins et al. 2006; Tobajas et al. 2016; Rao and Satayanarayana 2019). However, uniaxial experiments do not provide sufficient information to accurately characterise these materials (Sasso et al. 2008). To propertly parameterize a model, a full suite of tests should be performed to span the full range of intended deformations. These may include biaxial, planar, and volumetric tests (Shahzad et al. 2015). However, performing such tests is time-consuming, laborious, and requires specialist equipment (cameras, load cells, instruments to deform materials, clamps, etc.) (Avanzini and Battini 2016). It is also complicated by the lack of standardised testing methods (Avanzini and Battini 2016; Makinde et al. 1992; Boehler et al. 1994). Additionally, each test typically requires a specific sample shape, and even minor difference in chemical compositions between samples can significantly alter their mechanical properties (Shahzad et al. 2015).

Having obtained a rich set of stress–strain data, the final step is to fit these data to a model, and iterate to find the best-fit material parameters, for the chosen form of model. To this end, researchers have recently begun to combine artificial neural networks (ANN) with optimisation algorithms (Tran et al. 2023; Sang-To et al. 2023; Ho et al. 2022; Sang-To et al. 2022; Minh et al. 2023). One recently used approach integrated ANN with balancing composite motion optimisation (BCMO) to address optimisation challenges and predict material properties (Tran et al. 2023). In another approach, an effective optimisation method was introduced for structural health monitoring

(SHM) in truss-like structures (Sang-To et al. 2023). In another research, to overcome damage modelling limitation, a coupled model named ALOANN, which combines an ANN with the antlion optimiser (ALO), is employed (Ho et al. 2022).

Firouzi (Firouzi 2022; Firouzi and Żur 2023) created a comprehensive framework for analysing the significant deformation of hyperelastic membranes, accounting for hysteresis and viscoelastic effects. Their paper introduces a theoretical formulation of self-healing variables, encompassing elastic modulus, shear modulus, Poisson's ratio, and bulk modulus. It proposes a new healing variable based on elastic stiffness recovery, in line with continuum damage-healing mechanics (Voyiadjis et al. 2020). Zili and colleagues proposed a novel smoothed particle hydrodynamics (SPH) technique designed to eliminate undesired distortions in the material stability domain (Dai et al. 2017). Yongchang Cai proposed a mixed cover meshless method (MCMM) to address elasticity and fracture problems (Cai et al. 2018). Nguyen employed non-uniform rational B-splines (NURBS) as the fundamental functions to approximate both the geometry and field variables in the governing integral equations. The study indicated that the IGA-SGBEM method achieved remarkably accurate results (Nguyen et al. 2017). Nguyen-Thanh et al. presented a parametric deep energy method (P-DEM) for elasticity problems accounting for strain gradient effects (Nguyen-Thanh et al. 2020, 2021). In another research work, the authors used a novel isogeometric analysis using polynomial splines over hierarchical T-meshes for two-dimensional elastic solids (Nguyen-Thanh et al. 2011).

This study introduces a new technique to identify the parameters of a particular constitutive relation. The technique is based on the integration of optical techniques with hybrid optimisation to identify the mechanical properties of rubber-like materials. The technique involves applying a rich set of inhomogeneous deformationsto a rectangular cuboid sample, which indices a wide variety of generally inhomogeneous stress and strain fields. Commercially available software was then used to optimise the sets of coefficients for a hyperelastic constitutive model in a single set of experiments.

In this study, three identification techniques were applied to identify the parameters of four commonly used hyperelastic constitutive relations of a commercially available and commonly used silicone: Ecoflex 00-50. The first technique was to perform traditional uniaxial tests on a dumbbell-shaped sample using uniaxial tests. Two other techniques were based on an optical system in which a rectangular cuboid sample was subjected to a rich set of strains by twisting, bending, and stretching (inhomogeneous deformation) and pure stretching (uniaxial optical) using a 6-degrees-of-freedom force-torque sensor. The hyperelastic model coefficients were separately identified under Instron-based uniaxial stresses, inhomogeneous deformation (IHD), and optical uniaxial deformation (OU).

To compare the performance of the constitutive relations and identified parameters obtained from the Instron uniaxial test, optical uniaxial test, and inhomogeneous deformation tests, a new set of experiments comprising four new different inhomogeneous deformations (validation deformation) were performed. The parameters obtained from the Instron uniaxial test, optical uniaxial test, and inhomogeneous deformation tests were then used to predict the validation deformations and compared to the validation deformations measured by the optical system to determine the most suitable method to estimate the mechanical properties of the material.

The novelties of this work includes the high accuracy profile fit providing accurate parameter estimates estimated parameters, and a new stereoscopic technique to identify the coefficients of hyperelastic constitutive relations under inhomogenous deformatins. The tool was developed at Auckland Bioengineering Institute (ABI) to obtain surface profiling accuracy up to the micrometre level.

2 Methods

2.1 Dumbbell sample preparation

A dumbbell sample was created (Smooth On Ecoflex 00-50) conforming to the ASTM D412 (Standard Test Methods for Vulcanized Rubber and Thermoplastic Elastomers—Tension 2022) standard with thickness of 6 mm. The same mass of Ecoflex 00-50 part A and Ecoflex 00-50 part B were poured into a container and mixed. The mixture was then left in a vacuum chamber to remove air bubbles

and, after air was removed, the degassed silicone was poured into an acrylic mould (Fig. 1 Left) and left at room temperature for 24 h to cure.

The experiments were conducted on a uniaxial material test device (Instron 5567) equipped with a 1 kN load cell, at a temperature of about 24 °C. A video extensometer was installed on the Instron machine and two dots were used on the sample to measure the extension of the sample (Fig. 1 Right). The tests performed in this manner on the Instron machine are referred to as Instron uniaxial (IU) tests in this study.

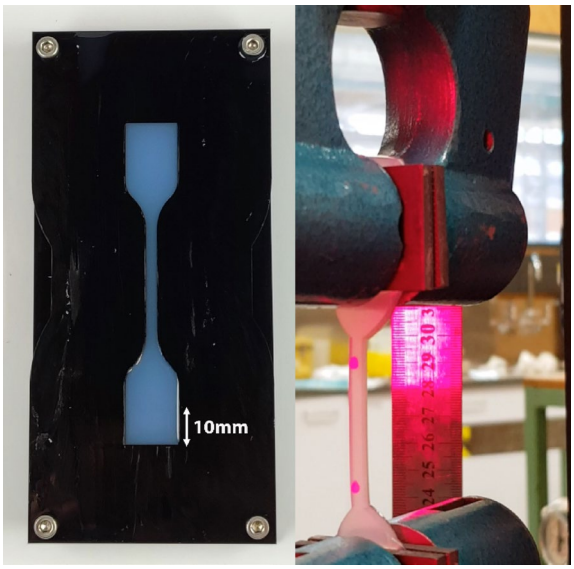

Fig. 1 The dumbbell sample. The picture on the left shows the Ecoflex 00-50 poured int the mould made from acrylic. The picture on the right depicts the specimen clamped in the Instron machine, and two red reference points are designated so that the Instron would track the points

2.2 Rectangular cuboid sample preparation

Ecoflex 00-50 (Smooth On Ecoflex 00-50) is one of the most commonly-used silicones in a wide variety of applications (Shivapooja et al. 2015; Roberts et al. 2013; Yap et al. 2016; Kim et al. 2016; Nasab et al. 2017; Ranzani et al. 2015). To maintain the simplified experiments, a rectangular cuboid sample was constructed from Ecoflex 00-50. The rectangular cuboid elastomer sample was cast in a three-dimensional (3D) printed polylactic acid (PLA) mould constructed using an Ultimaker 2+3D printer (Ultimaker 2+3D printer 2022). Two-part silicone (Ecoflex 00-50) was used with equal parts A and B by mass, as recommended by the manufacturer. These were mixed and degassed in a vacuum chamber to remove trapped air and then poured into the mould. After curing at room temperature for 24 h, the sample was taken out of the mould. (Fig. 2A). The rectangular cuboid was 30 mm long with a square cross-section with a 15 mm edge (Fig. 2B).

A black microdot pattern was used to enable surface tracking, so that surface deformation could be compared the with the result of FE models (Fig. 2C). The microdot pattern was inked onto the surface of the rectangular cuboid on all sides using acrylic ink spots, 200 µm to 300 µm in diameter. These microdots provided simply identifiable markers that were manually reconstructed throughout the 3D deformation experiments to generate a gold standard set of material points that can be used to measure the FE model error. A polyethylene terephthalate film stencil was used to obtain an even distribution of the microdots across all the rectangular cuboid surfaces. The stencil comprised a 3×5 grid of evenly spaced laser-cut holes with 4 mm spacing between the centres of the microdots.

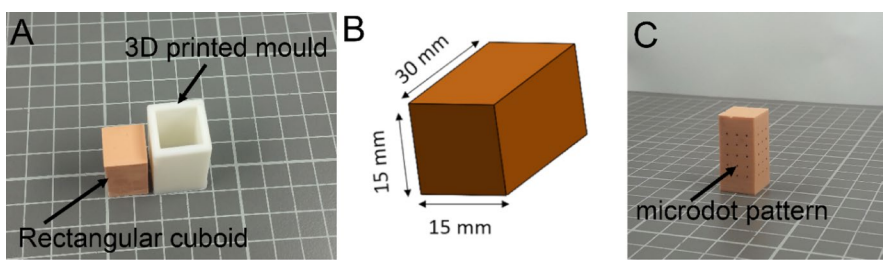

Fig. 2 **A** A photograph of the 3D printed mould used to manufacture the rectangular cuboid. **B** The dimension of the rectangular cuboid sample. **C** microdot patterns used to compare the 3D displacement measurement with the FE models

2.3 Surface deformation measurement

Both sides of the sample were glued to PLA bases using Sil-Poxy (Smooth-On, Inc.). One side was held in a fixed position. The other side was connected to a force-torque transducer (nano 17, ATI Industrial Automation). The force-torque sensor was manually moved into eight different configurations to induce a range of strain fields within the sample, including tensile, compression, torsion, and shear strains. The six components of the reaction force/torque were measured for each configuration (Fig. 3).

Surface deformation was measured using a stereoscopic system consisting of eight USB 3.0 CMOS cameras (Flea3 FL3-U3-13Y3M, Point Grey Research Inc., Canada), each equipped with 6 mm lenses (Fujinon Lens DF6HA-1B, Fujifilm Corporation, Japan). Circular polarisers (PL-CIR S 27 mm/0.75, Hoya Corporation, Japan) were attached to each lens to reduce specular reflections. Four cameras were mounted at 45° on acrylic blocks at the four corners of a rectangular aluminium optical breadboard with sides approximately 225 mm and 150 mm to cover two sides of the sample simultaneously. Four other cameras were mounted at 45° on acrylic blocks in the middle of the rectangular optical breadboard, directly pointed at one side of the sample (Fig. 3). Software-triggered image acquisition was performed in LabVIEW 2019 (National Instruments, USA) at a rate of one capture per deformation. Surface illumination was provided by four green (560 nm) light-emitting diodes (LEDs), mounted between the corner cameras. The cameras' intrinsic and extrinsic parameters were identified using a multi-camera calibration technique, which automatically calculates parameters from sets of calibration images of a checkerboard pattern (HajiRassouliha 2017).

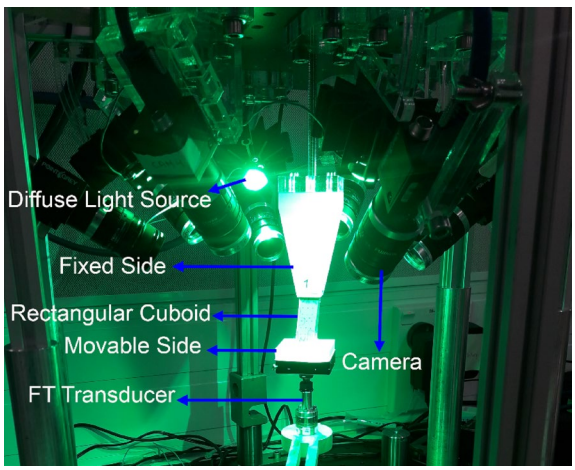

Fig. 3 FT transducer performing arbitrarily moving on a rectangular cuboid silicone sample made from Ecoflex 00-50. The FT transducer records the 3D force vector during the displacement, while cameras capture images from eight different views at each step

2.3.1 Surface profiling

The calibrated stereoscope system was used to reconstruct the 3D geometry by integrating the overlapping views of at least three cameras. The method developed by HajiRassouliha et al. (2013) for surface profiling was used to calculate the sample deformation. Based on this method, we applied biquadratic polynomial transformations to two views to align with a third camera, known as the reference camera, for each side of the sample.

At each pair view (the overlapping view of two cameras), approximately 30 distinct points were matched as an initial estimate of the surface deformation. At each deformation, each side of the sample was 3D reconstructed to obtain the whole volume of the sample for each deformation. The pre-deformation state was considered as the reference, shown by blue dots in (Fig. 4), and the displacement at each step was measured by comparing the coordinate with the reference state. Detailed information on the 3D reconstruction is explained in HajiRassouliha et al. (2018).

The sample was submitted to two different deformation configurations for coefficient optimisation, and an arbitrary deformation configuration for the test and validation. The first configuration included eight different arbitrary movements that induced a mix of tensile, compression, shear, and torsion in the sample referred to as inhomogeneous deformation test. The other experimental configuration was a simple uniaxial test performed on the sample and stretched to eight different lengths.

Once the hyperelastic model coefficient was determined using each deformation configuration (i.e. inhomogeneous deformation and uniaxial deformation), an experiment comprising four arbitrary deformations was performed to evaluate the suitability

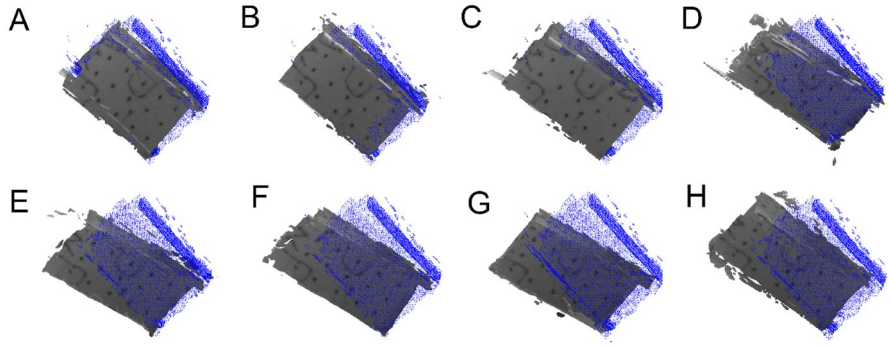

Fig. 4 The 3D reconstructed point cloud for eight different steps of the inhomogeneous deformation configuration, compared to the reference state designated in blue dots

of the determined hyperelastic constitutive model coefficient.

2.4 Hyperelastic models

Studies have used a wide variety of hyperelastic constitutive models to describe the mechanical behaviour of Ecoflex 00-50. Hyperelastic constitutive models for rubbers and rubber-like materials can be loosely categorised into phenomenological models such as Ogden and Yeoh, and micromechanical network models such as Arruda-Boyce (He et al. 2021).

According to the literature (Elsayed et al. 2014; Zhang et al. 2021; Sarkar et al. 2019; Shivapooja et al. 2015; Sparks et al. 2015), the Ogden N1, third order Ogden (Ogden N3), Yeoh, and Arruda-Boyce are common candidates for defining the mechanical behaviour of Ecoflex 00-50. However, there is still uncertainty about which constitutive model is the most appropriate for characterising Ecolfex 00-50. In this paper we compared Ogden N1, Ogden N3, Yeoh, and Arruda-Boyce hyperelastic constitutive models to determine how well they describe the behaviour of Ecoflex 00-50. These constitutive models are briefly described below.

2.4.1 Ogden model

The Ogden model calculates the strain energy function based on the principal stretches (λ_1, λ_2, λ_3), with the incompressibility constraint $\lambda_1\,\lambda_2\,\lambda_3 = 1$. A notable advantage of principle stretches is that they are directly measurable quantities (Chang et al. 1991). The relation of the Ogden strain energy potential is defined by:

$$U = \sum_{i=1}^{N} \frac{2\mu_i}{\alpha_i^2}\left(\lambda_1^{a_i} + \lambda_2^{a_i} + \lambda_1^{-a_i}\lambda_2^{-a_i} - 3\right) \tag{1}$$

where λ_i is the principle stretches and μ_i and α_i are constants that determine the material's behaviour.

2.4.2 Yeoh model

The Yeoh strain energy function is based on the first invariant, and the strain energy density for this model for an incompressible material is written as:

$$U = \sum_{i=1}^{3} C_{i0}(I_1 - 3)^i \tag{2}$$

The initial shear module for the Yeoh model is given by: $\mu_0 = 2C_{10}$ and $I_1 = \lambda_1^2 + \lambda_2^2 + \lambda_1^{-2}\lambda_2^{-2}$.

2.4.3 Arruda-Boyce model

The Arruda-Boyce model is based on the behaviour of molecular chain networks. In this model, the strain energy is assumed to be equal to the sum of the strain energies of individual chains that are randomly oriented in 3D space (Arruda and Boyce 1993). The model for an incompressible material is described as:with

$$U = \mu \sum_{i=1}^{N} \frac{C_i}{\lambda_m^{2i-2}}\left(\bar{I}_1^i - 3^i\right)$$

$$C_1 = \frac{1}{2}, C_2 = \frac{1}{20}, C_3 = \frac{11}{1050}, C_4 = \frac{19}{7000}, C_5 = \frac{519}{673750} \tag{3}$$

where $\bar{I}_1 = I_1(\det(F))^{\frac{-2}{3}}$, F is the deformation gradient, and $N = 5$.

μ is the initial shear modulus, and λ_m is the stretch at which the polymer network becomes locked and there is a significant upturn in the stress–strain curve.

2.5 Hybrid optimisation techniques

Hybrid optimisation is a popular approach that combines multi-optimisation techniques to take advantage of the distinct strengths of each approach. We used a genetic algorithm (GA), a derivative-free optimisation method (Deb and Goel 1993), to find the global minimum. At the minimum determined by the GA, the optimisation continued by a quasi-Newton sequential quadratic programming (SQP) method to estimate a well-conditioned minimum in the vicinity of the unique optimum. The performance of quasi-Newton algorithms relies on the initial estimates, whereas heuristic algorithms are less affected by these initial values. While heuristic algorithms are effective in identifying the vicinity of minimum values, quasi-Newton methods are preferred when precise determination of the minimum within a constrained domain is required.

2.5.1 *Objective function*

The objective function (known as a fitness function in GA and cost function in SQP) is defined in this study as the sum of squared errors between model predictions and the corresponding surface profiling data. A box constraint was applied to the optimisation describing each parameter's upper and lower limit bounds (Table 1). The limits were selected in all orientations so at the lower limit, the model was softer than the silicone phantom, and at the upper limit, the model was stiffer than the silicone phantom.

The nonlinear least-squares objective function ϕ is defined as:

Table 1 The Optimisation boundary limit for the coefficients of all four employed hyperelastic constitutive models

Constitutive model	Coefficient 1 (kPa)	Coefficient 2
Ogden N1	$-100 < \mu_1 < 100$	$-1 < \alpha < 3$
Ogden N3	$-20 < \mu_i < 20$	$1 < \alpha_i < 8$
Yeoh	$-10 < C_{i0} < 50$	NA
Arruda-Boyce	$1 < \mu < 100$	$-1 < \lambda < 8$

$$\phi = \sum_{j=1}^{M} \sum_{i=1}^{N_j} \left\| Z_{ij} \right\|^2 \tag{4}$$

where the $\left\| Z_{ij} \right\|$ is the Euclidean distance between ith data point on the sample and the corresponding point on the model's surface in the jth experiment. N_j is the number of control points measured at each surface profiling in the jth experiment, and M is the total number of experiments conducted. The root-mean-square error (RMSE) is defined as:

$$RMSE = \sqrt{\frac{\sum_{j=1}^{M} \sum_{i=1}^{N_j} \left\| Z_{ij} \right\|^2}{\sum_{j=1}^{M} N_j}} \tag{5}$$

2.5.2 *Optimisation procedure*

The optimisation procedure was implemented in MATLAB (Version 2018b, The MathWorks Inc., USA) and performed in two phases (Fig. 5). The objective function was evaluated by solving the FE model in a commercially available FE package, Abaqus. Two termination conditions were used at each phase: (1) if the RMSE was less than 0.05 mm, which was sufficient for the purpose of this study and could avoid excessive search time, (2) the step tolerance of the optimisation was less than 10^{-12}. The algorithm would terminate the optimisation if either of the termination condition is satisfied at each phase.

In phase-I (Fig. 5 left), the hyperelastic constitutive model coefficients were estimated for each iteration using a GA where intermediate crossover and adaptive mutation were used to elicit the next generation of parents. The crossover fraction was set to 0.8, and the crowding technique was used as the distance measure during the GA optimization process. Once phase-I was finished, phase-II (Fig. 5 right) used the SQP optimisation from the optimum measured by the GA in phase-I. For detailed information about the SQP algorithm, the reader is referred to Schittkowski (1985), Han (1977). Phase-II searched for the optimum in the vicinity of GA optimum to improve the local minimum estimate. It also calculated the parameter estimates' local conditioning (i.e. Hessian matrix, gradient).

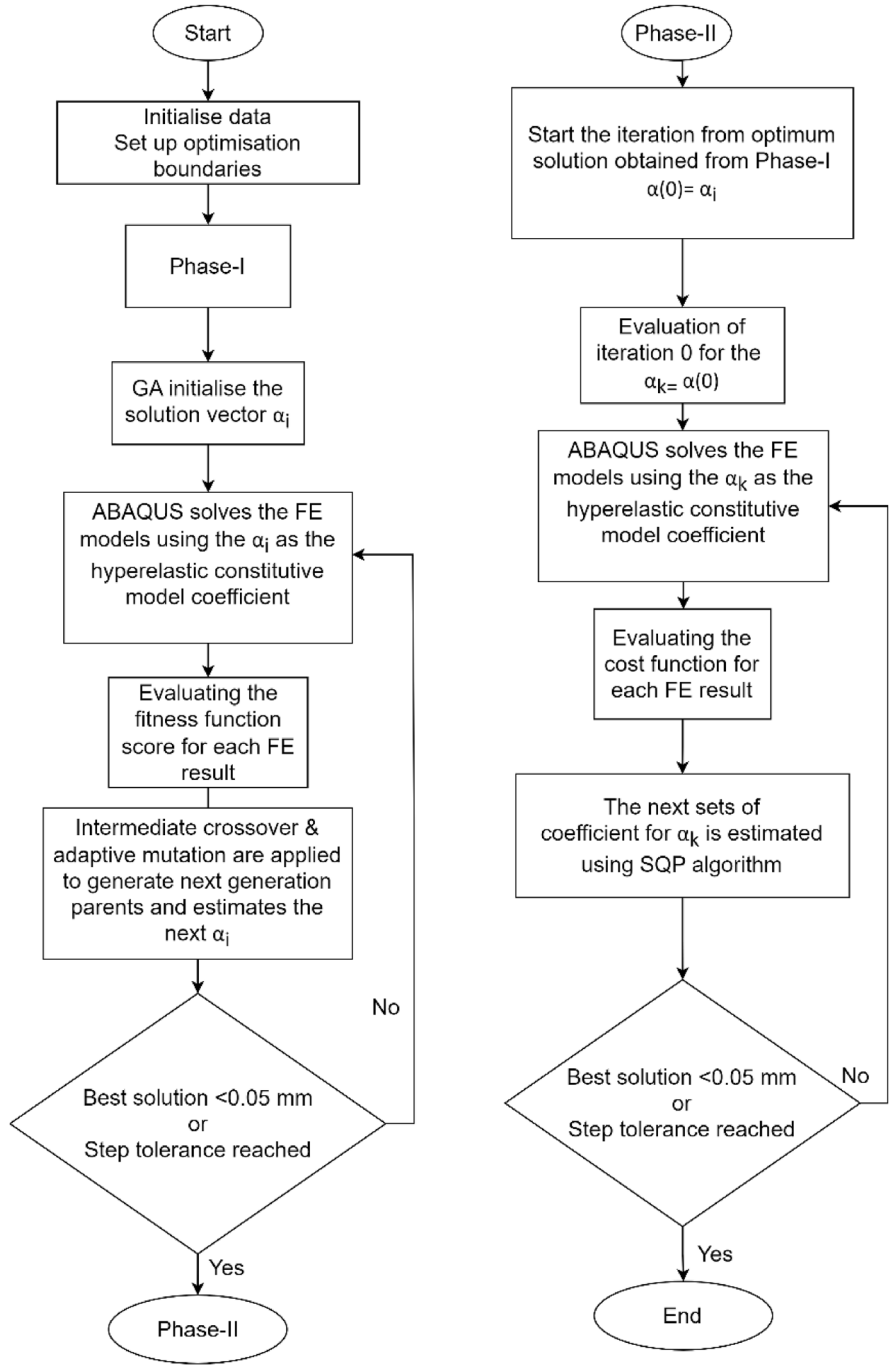

Fig. 5 Optimisation flowchart shows the two-phase optimisation method for optimising the coefficients of each hyperelastic constitutive model. Phase-I depicts the steps to find the minimum solution. A gradient-based optimisation follows it in phase-II to locate the well-conditioned optimum solution and generate a Hessian matrix at the optimum solution to determine the behaviour of the function at the optimum solution

2.5.3 Determinability

The Hessian matrix ($\boldsymbol{H_0}$) in the vicinity of the optimum set of parameters was used to evaluate the determinability of the models (Sorooshian et al. 1982; Mh and Gm 1985). This area is known as the confidence or the indifference region, and is a hyperellipsoid in optimisation parameter space. A small deviation on the parameter vector ($\delta\theta$) will result in a change in the objective function ($\delta\Phi$), defined as:

$$\delta\phi = \delta\theta^T H_0 \delta\theta \tag{6}$$

We used three criteria to assess the hyperellipsoid region. In order of importance (Gamage et al. 2011): The determinant of the Hessian, det ($\boldsymbol{H_0}$) or also known as D-optimality criterion; the condition number of the Hessian, cond ($\boldsymbol{H_0}$); and the M-optimality criterion, det ($\widetilde{\boldsymbol{H}}_0$).

- The D-optimality criterion indicates the volume of the indifference region, which ideally should be small, demonstrating a small variance of all parameters. Due to the inverse relation between the volume of indifference region and det ($\boldsymbol{H_0}$), to obtain this, the det ($\boldsymbol{H_0}$) should be maximised.
- The cond ($\boldsymbol{H_0}$) represents the eccentricity or the ratio of the longest to the shortest hyper-ellipsoidal axis which is inversely proportional to the eigenvalues of $\boldsymbol{H_0}$. cond ($\boldsymbol{H_0}$), is a measure of the disparity between the smallest and largest determined linear combination of the parameters.
- The M-optimality criterion is calculated using:

$$\det(\tilde{\boldsymbol{H}}_0) \text{ where } \tilde{H}_{ij} = \frac{H_{ij}}{\sqrt{H_{ii}H_{jj}}} \text{ (i, and j are not summed)} \tag{7}$$

M-optimality illustrates the alignment of each two hyper-ellipsoid axis along the reference axes, and the angle formed by the elliptical and reference axes generally describes the degree of interaction among the two relevant parameters. The value of one means there is no interaction between the parameters and thus shows a perfect alignment between the elliptical axes and material parameters axes.

It should be noted that the determinability criterion is not an indication of the accuracy of the predicted optimum values. However, they indicate the relative confidence in parameters at the optimum values.

3 Results

The results section comprises three main sections. The first section shows the hyperelastic constitutive relations coefficients obtained from IU test data. The second section includes the hybrid optimisation results for each hyperelastic constitutive relation. The third section compares the hyperelastic constitutive model coefficients calculated from IU, OU, and IHD experiments.

3.1 Instron uniaxial test

The commercially available FE package, Abaqus, was used to identify the parameters of the hyperelastic constitutive relations from IU test data. The calibration was performed for Ogden N1, Ogden N3, Arruda-Boyce, and Yeoh hyperelastic constitutive models to determine the parameters for each model. The coefficients of the constitutive relation were determined through a least-squares-fit procedure, which minimised the relative error between the stress calculated by the hyperelastic constitutive model and experimental data. For the n engineering-stress and strain data pairs, the relative error was measured from:

$$E = \sum_{i=1}^{n} \left(1 - \frac{T_i^{th}}{T_i^{\text{test}}}\right)^2 \tag{8}$$

where T_i^{test} is a stress value from the test data, and T_i^{th} comes from one of the nominal stress expressions derived from the hyperelastic constitutive model (Table 2).

Fitting each hyperelastic model to the IU test data is shown in Fig. 6. The Ogden N3, had the highest performance with 0.335 fitting error, and the fitting error for Yeoh, Arruda-Boyce, and Ogden N1, was 1.712, 2. 936, and 4.584 respectively.

Thus, the IU test results suggest that Ogden N3 was the most accurate hyperelastic model for describing the Ecoflex 00-50 stress–strain behaviour.

Table 2 The hyperelastic constitutive model coefficients estimated based on Instron uniaxial test

Model name	Optimised coefficient (kPa)
Ogden N1	$\mu = 31.003$ $\alpha = 0.043891$
Ogden N3	$\mu_1 = 12.116$, $\mu_2 = 10.856$, $\mu_3 = -2.8631$ $\alpha_1 = 3.3483$, $\alpha_2 = 4.0877$, $\alpha_3 = 5.1991$
Yeoh	$C_{10} = 7.355$, $C_{20} = 10.519$, $C_{30} = 6.14$
Arruda-Boyce	$\mu = 23.878$ $\lambda_c = 4.8253$

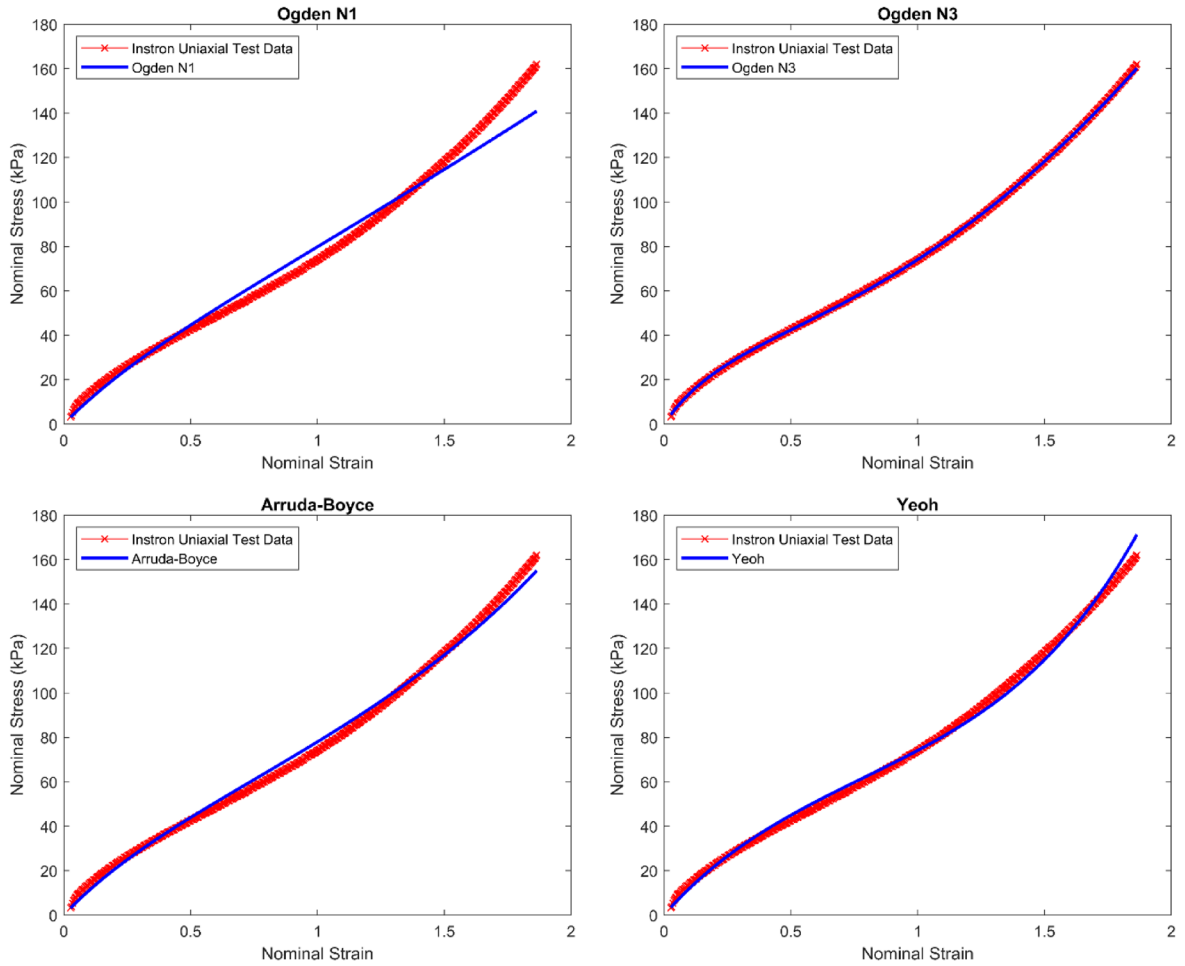

Fig. 6 The estimated stress by each hyperelastic models and compared with the stress recorded from IU tests

3.2 Hybrid optimisation

This section considers the parameter estimates obtained through each experiment's hybrid optimisation algorithm. The error is defined as the RMS discrepancy between the experimental surface deformation and the FE model. For each hyperelastic constitutive model optimisation, the average error for all models is reported, and determinability information for each model was calculated. This study shows the average M-optimality for combining all parameters for the hyperelastic constitutive relations. Figure 7 provides a visual depiction of the Ogden N3 optimised model results for the inhomogeneous deformation and illustrates the discrepancy with the corresponding points obtained from experimental surface profiling.

Figure 8 illustrates the convergence of the hybrid optimisation method for Ogden N3, and the integration of the SQP algorithm with GA occurred at approximately iteration 450.

3.2.1 Inhomogeneous deformation experiments

The inhomogeneous deformation included uniaxial stretch, shear, and torsion. The results listed in Table 3 show that Ogden N3 had the lowest RMS error (0.574 mm) among all evaluated hyperelastic constitutive models, and Ogden N1, Yeoh, and Arruda-Boyce had larger RMS errors, with the

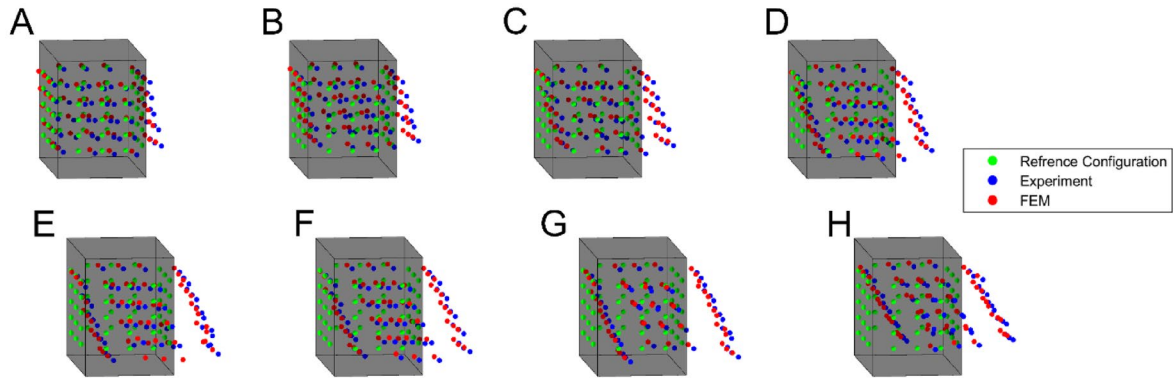

Fig. 7 A visual representation of the error between the deformation measured by the Ogden N3 optimised result (red dots) and the experiment data (blue dots) for the complex stress deformation, eight in total. The green dots depict the sample at the reference state (i.e. the reference of each blue and red dot)

magnitudes 0.615 mm, 0.639 mm, and 0.643 mm, respectively. There was no significant difference between the average error measured by Yeoh and Arruda-Boyce hyperelastic models. Furthermore, various heuristic methods, including particle swarm optimisation (PSO) and simulated annealing (SA), were evaluated in comparison with GA for Ogden N3. The results clearly indicate that GA yields lower RMS error compared to the other methods. Specifically, the RMS error obtained with PSO and SA were 0.576 mm and 0.587 mm, respectively, both of which are greater than the RMS error estimated with GA.

Ogden N3 had the smallest indifference region volume since it had the largest D-optimality of 0.487, which shows that, within this region, the objective function would not increase more than ($\delta\Phi$) and indicates relatively small variance in the parameters. Therefore, the parameters space is relatively sensitive to the parameters' choice compared to the other constitutive models. In contrast, Ogden N1 had a relatively large indifference region volume, with a D-optimality of 0.004, indicating relatively large variance; thus, the parameter space is relatively insensitive to the selection of the parameters.

The Ogden N3, and Ogden N1 had the same condition number of $\boldsymbol{H_0}$, cond ($\boldsymbol{H_0}$), with the value of 333.333 and Arruda-Boyce had the smallest condition number value with the magnitude of the 2.058 (Table 3). Based on the definition of the condition number, as the cond ($\boldsymbol{H_0}$) approaches unity, the axes of the indifference ellipsoid approximate to the same length (circle/hyper-sphere), and changes in all directions in the parameter space is equally accessible (The distance between each parameters on the axis and the origin is the same). As cond ($\boldsymbol{H_0}$) is significantly more than 1, this indicates that the indifference ellipsoid is larger in one direction, and the variation in all directions in the parameter space is unequally accessible. Therefore, for the Arruda-Boyce model,

Table 3 The hyperelastic constitutive model parameters optimisation result using the Inhomogeneous experiments

Model name	Optimised coeffient (kPa)	Average error (mm)	Det (H_0)	Cond (H_0)	M-optimality
Ogden N1	$\mu=20.3\ \alpha=0.5234$	0.612	0.004	333.333	0.993
Ogden N3	$\mu_1=5.473, \mu_2=-2.63, \mu_3=10.687$ $\alpha_1=6.6034, \alpha_2=2.142, \alpha_3=2.6814$	0.574	0.487	333.333	0.017
Yeoh	$C_{10}=6.9151, C_{20}=3.0667\ C_{30}=3.9378$	0.639	0.284	10.417	0.337
Arruda-Boyce	$\mu=16.9\ \lambda=5$	0.643	0.416	2.058	0.054

The result indicates that Ogden N3 had the lowest error and had the largest indifference region according to the D-optimality criterion

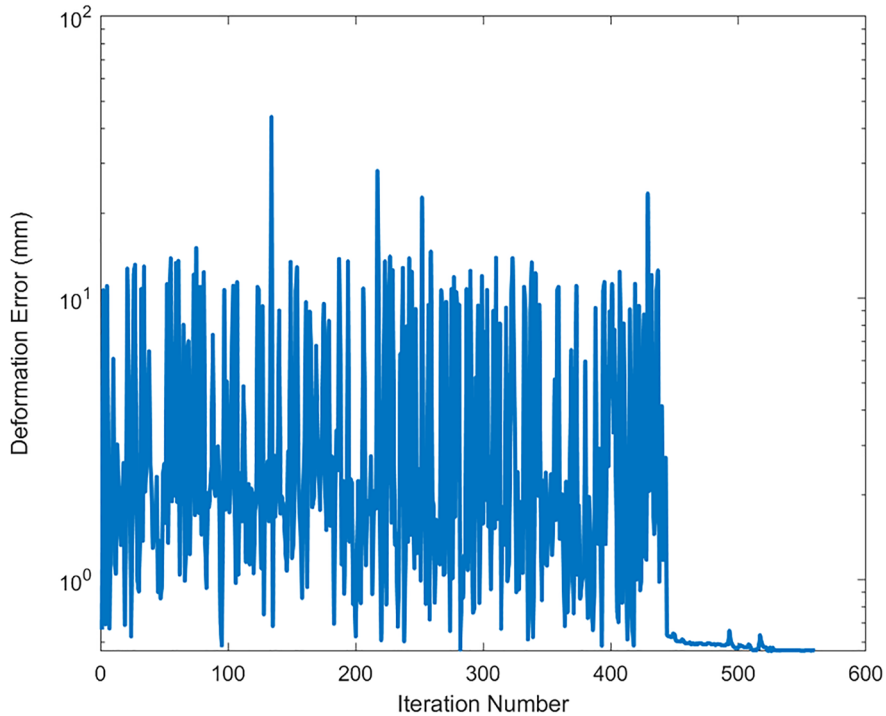

Fig. 8 Hybrid optimisation graph showing the result of integration of SQP with GA for Ogden N3

the parameter space is more equally accessible than the Ogden model.

M-optimality describes the interaction between the parameters of the hyperelastic constitutive model. The M-optimality of optimisation results (Table 3) indicates that the Ogden N1 had the lowest interaction between the parameters (0.993). The Ogden N3 had the highest interaction between the parameters (0.017). The interaction between the parameters for the Arruda-Boyce model was also relatively high (0.054) to estimate the optimum results.

3.2.2 Uniaxial experiments

The hyperelastic constitutive model parameters optimisation results are based on the uniaxial experiments reported in (Table 4). Ogden N3 had the best performance and lowest error in the uniaxial experiment optimisation, similar to the inhomogeneous deformation. The Ogden N3 had an error of 0.559 mm, with the next lower errors for the Arruda-Boyce model, Ogden N1 model, and Yeoh model of 0.642 mm and 0.664 mm and 0.679, respectively.

Ogden N3 had the largest indifference region with the D-optimality of 5.204. Ogden N1 followed with

Table 4 The hyperelastic constitutive model parameters optimisation result using the uniaxial stress experiments

Model name	Optimised coefficients (kPa)	Average error (mm)	Det (H_0)	Cond (H_0)	Average M-optimality
Ogden N1	$\mu = 31.003$ $\alpha = 0.043891$	0.664	2.639	2.924	−0.067
Ogden N3	$\mu_1 = 12.116$, $\mu_2 = 10.856$, $\mu_3 = -2.8631$ $\alpha_1 = 3.3483$, $\alpha_2 = 4.0877$, $\alpha_3 = 5.1991$	0.559	5.204	20.8333	0.18
Yeoh	$C_{10} = 7.355$, $C_{20} = 10.519$ $C_{30} = -6.14$	0.679	1.965	2.717	0.237
Arruda-Boyce	$\mu = 23.878$ $\lambda_m = 4.8253$	0.624	1.914	20.408	0.801

The result indicates that Ogden N3 had the lowest error and had the largest indifference region accordion to the D-optimality criterion

the smallest indifference region with the D-optimality of 2.639, and then Yeoh, and Arruda-Boyce with the 1.965, and 1.914, respectively. This indicates that for the Ogden N3 there is a relatively small variance in the parameters. Thus, the parameter space is relatively sensitive to the choice of the parameters compared to the other evaluated hyperelastic models.

The Ogden N3 and Arruda-Boyce had almost the same condition number of $\boldsymbol{H_0}$, cond ($\boldsymbol{H_0}$), with values 28.833 and 20.408, respectively. The cond ($\boldsymbol{H_0}$) value for Ogden N1, and Yeoh was 2.924, and 2.717, respectively. The cond ($\boldsymbol{H_0}$) shows that the change the in parameters for Ogden N3 and Arruda-Boyce in all directions is relatively less equally accessible compared to the Ogden N1 and Yeoh (Table 4).

According to the M-Optimality criterion, the interaction between the Arruda-Boyce parameters was the smallest (0.801), and the interaction between the Ogden N1 parameters was the highest (-0.067). The interaction between the parameters for Ogden N3 (0.18) was smaller than the Ogden N1, and for Yeoh the interaction (0.237) was smaller than Ogden N3 (Table 4).

3.3 Optimisation result comparison

The coefficients of the constitutive relations for different hyperelastic constitutive models have been calculated through (1) parameter optimisation of inhomogeneous; (2) parameter optimisation of optical uniaxial experiments; and (3) identifying the data based on Instron uniaxial tests. In order to validate each technique and determine the accuracy of each hyperelastic coefficient of the constitutive relation, the rectangular cuboid sample was subjected to four new inhomogeneous deformations. FE model predicted the surface deformation of the sample using the identified hyperelastic constitutive relations coefficients. Finally, FE surface deformation results were compared against the 3D surface deformation results obtained from four new inhomogeneous deformation experiments. The data in Table 5 shows the average error result for comparing the deformation measured using each technique for calculating the material constants of hyperelastic constitutive models against the experimental deformation.

This results demonstrate that the deformation comparison error calculated using the parameters obtained from inhomogeneous deformation was significantly smaller than the error calculated using two other techniques for all hyperelastic constitutive models (Table 5). The parameters obtained from inhomogeneous deformation for Ogden N3 had the best performance with 0.593 mm average error. Yeoh with 0.741 mm had the second-best performance, and Arruda-Boyce and Ogden N1 had the third and fourth accuracy with average errors of 0.823 mm and 0.882 mm, respectively. The average error result using the hyperelastic constitutive model parameter obtained from the uniaxial experiment optimisation had the same order of accuracy as the inhomogeneous deformation parameters. Among the results obtained using the uniaxial coefficient, Ogden N3 had the best performance with a 1.039 mm error and Ogden N1 had the highest measured error with 1.426 mm. The Instron uniaxial based parameters had the lowest accuracy with different sequences. The best performance was for Ogden N3 with 1.365 mm error, and then Ogden N1, Arruda-Boyce, and Yeoh had the lowest error, respectively with 1.491 mm, 1.496 mm, and 1.520 mm.

Table 5 The average error on the unseen experiment that comprised arbitrary movement of sample for the different hyperelastic constitutive model based on the parameters obtained from inhomogeneous deformation (IHD) optimisation and optical uniaxial (OU) optimisation experiments, and Intron uniaxial (IU) test

Model	IHD average error (mm)	OU average error (mm)	IU average error (mm)
Ogden N1	0.882	1.426	1.491
Ogden N3	0.593	1.039	1.365
Yeoh	0.741	1.276	1.520
Arruda-Boyce	0.823	1.375	1.496

4 Discussion

In this study, we proposed an optically-based surface profiling method and hybrid optimisation technique to identify the coefficients for a range of hyperelastic constitutive relations. The stereoscopic 3D reconstruction results were used as the benchmark results to compare the predictive power of identifying hyperelastic model parameters using inhomogeneous deformation tests, optical uniaxial test and Instron uniaxial tests. The new optical technique used a simple

rectangular cuboid sample that undergoes a series of inhomogeneous strains (shear, torsion, uniaxial, etc.) in response to the imposition of relatively simple boundary forces and torques. Using a finite element model of the experimental tests, with the experimentally measured boundary forces and torques imposed on the model, a hybrid optimisation was performed to identify the hyperelastic constitutive model parameters that best match the model predictions of free surface deformations to those measured experimentally. Three separate experiments were conducted to identify the hyperelastic constitutive model parameters. One experiment comprised inhomogeneous deformations (uniaxial, shear, torsion, etc.), the second experiment comprised only optical uniaxial deformations, and the third experiment was traditional dumbbell shape uniaxial test using Instron machine. Performing the optimisation for both optical experiment data sets, and calibrating the coefficients of the constitutive relations for Instron uniaxial data sets using Abaqus, indicated that the parameters estimated from inhomogeneous deformations yielded parameters that provided more accurate results than those parameters estimated from only uniaxial experiments.

The determinability study performed on various models showed that, at the optimum parameter estimates, the indifference region (D-optimality) was smaller for the parameters obtained from only optical uniaxial deformations (Table 4) compared to the parameters measured from inhomogeneous deformations (Table 3). These findings indicate that the indifference region of the identified parameters based on the optical uniaxial optimisation was larger than the indifference region of the identified parameters based on the inhomogeneous deformation configuration optimisation. This difference in the indifference region occurs since, in optical uniaxial optimisation, the parameters should only describe the strain-uniaxial stress curve, whereas for the inhomogeneous deformation configuration optimisation, the parameters should be valid for describing all existing types of strain–stress curves. Thus, the calculation of the parameters for the uniaxial optimisation a wider range of parameters can only define the uniaxial behaviour of the material.

The optimised parameters for all hyperelastic constitutive relations were obtained from optical and Instron uniaxial tests and inhomogeneous deformation experiments using a deformed sample from Ecoflex 00-50. In these tests the Ogden N3 parameters obtained from inhomogeneous deformation experiments provided the best accuracy (Table 5). This work indicates that hyperelastic constitutive model parameters obtained from the purely uniaxial experiments yield less accurate parameter estimates than those obtained from inhomogeneous deformation experiment.

5 Conclusions

This study introduced a new technique based on an optical deformation measurement system and hybrid optimisation to estimate hyperelastic constitutive model parameters for elastomeric materials using a single rectangular cuboid as a sample. The study demonstrated that a single uniaxial experiment is insufficient to estimate parameters for hyperelastic constitutive models when subjected to multiple types of stress, and the parameters calculated from inhomogeneous deformation provide more accurate FE predictions. Based on this study, hyperelastic constitutive parameter identification for applications with inhomogeneous strains should be carried out under inhomogeneous deformation tests instead of uniaxial tests. Doing so improves the FE modelling prediction accuracy where the materials undergo inhomogeneous deformation. This study demonstrated that a single series of inhomogeneous deformations are sufficient for reliable hyperelastic constitutive relation coefficient identification. The FE study demonstrated that the Ogden N3 relation provides more accurate results than other hyperelastic constitutive relations. The research faced two primary limitations. Firstly, the 3D reconstruction algorithm encountered challenges in accurately reconstructing the edges. Secondly, the hyperelastic material used in the study had to comply with the requirement of being incompressible.

Author contributions SM: Preparing the codes and conducting the experiments. Developing the method, analysis of the results and writing of the manuscript. DB: Advice on the concept, data analysis, and review of the manuscript. AT: Advice on the concept, data analysis, and review of the manuscript. PN: Advice on the concept, data analysis, and review of the manuscript.

Funding Open Access funding enabled and organized by CAUL and its Member Institutions. The study was funded by the University of Auckland.

Data availability The data are available upon request from the corresponding Author (i.e. SM).

Declarations

Conflict of interest There is no known conflict of interest for this work.

Ethical approval Not applicable.

References

Amin, A.F.M.S., Lion, A., Sekita, S., Okui, Y.: Nonlinear dependence of viscosity in modeling the rate-dependent response of natural and high damping rubbers in compression and shear: Experimental identification and numerical verification. Int. J. Plast. **22**(9), 1610–1657 (2006). https://doi.org/10.1016/J.IJPLAS.2005.09.005

Anssari-Benam, A.: On a new class of non-Gaussian molecular-based constitutive models with limiting chain extensibility for incompressible rubber-like materials. Math. Mech. Solids. **26**(11), 1660–1674 (2021). https://doi.org/10.1177/10812865211001094

Arruda, E.M., Boyce, M.C.: A three-dimensional constitutive model for the large stretch behavior of rubber elastic materials. J. Mech. Phys. Solids **41**(2), 389–412 (1993). https://doi.org/10.1016/0022-5096(93)90013-6

Avanzini, A., Battini, D.: Integrated experimental and numerical comparison of different approaches for planar biaxial testing of a hyperelastic material. Adv. Mater. Sci. Eng. (2016). https://doi.org/10.1155/2016/6014129

Bergström, J.: Elasticity/Hyperelasticity. In: Mechanics of Solid Polymers, pp. 209–307. William Andrew Publishing, Norwich (2015)

Boehler, J.P., Demmerle, S., Koss, S.: A new direct biaxial testing machine for anisotropic materials. Exp. Mech. **34**(1), 1–9 (1994). https://doi.org/10.1007/BF02328435

Boyce, M.C., Arruda, E.M.: Constitutive models of rubber elasticity: a review. Rubber Chem. Technol. **73**(3), 504–523 (2000). https://doi.org/10.5254/1.3547602

Bustamante, R., Rajagopal, K.R.: A new type of constitutive equation for nonlinear elastic bodies Fitting with experimental data for rubber-like materials. Proc. R. Soc. A **477**(2252), 20210330 (2021). https://doi.org/10.1098/RSPA.2021.0330

Cai, Y., Sun, P., Zhu, H., Rabczuk, T.: A mixed cover meshless method for elasticity and fracture problems. Theor. Appl. Fract. Mech. **95**, 73–103 (2018). https://doi.org/10.1016/j.tafmec.2018.01.011

Chang, T.Y.P., Saleeb, A.F., Li, G., Chang, T.Y.P., Saleeb, A.F., Li, G.: Large strain analysis of rubber-like materials based on a perturbed Lagrangian variational principle. CompM **8**(4), 221–233 (1991). https://doi.org/10.1007/BF00577376

Dai, Z., Ren, H., Zhuang, X., Rabczuk, T.: Dual-support smoothed particle hydrodynamics for elastic Mechanics. Int. J. Comput. Methods **14**(04), 1750039 (2017). https://doi.org/10.1142/S0219876217500396

Dal, H., Açıkgöz, K., Badienia, Y.: On the performance of isotropic Hyperelastic constitutive models for rubber-like materials: a state of the art review. Appl. Mech. Rev. (2021). https://doi.org/10.1115/1.4050978

Deb, K., Goel, T.: Controlled elitist non-dominated sorting genetic algorithms for better convergence. Lect. Notes Comput. Sci. (Incl. Subser. Lect. Notes Artif. Intell. Lect. Notes Bioinf.) **1993**, 67–81 (2001). https://doi.org/10.1007/3-540-44719-9_5

Dobrynin, A.V., Carrillo, J.M.Y.: Universality in nonlinear elasticity of biological and polymeric networks and gels. Macromolecules **44**(1), 140–146 (2010). https://doi.org/10.1021/MA102154U

Elsayed, Y., et al.: Finite element analysis and design optimization of a pneumatically actuating silicone module for robotic surgery applications. Soft Robot. **1**(4), 255–262 (2014). https://doi.org/10.1089/soro.2014.0016

Firouzi, N.: Mechanics of nonlinear visco-hyperelastic-hysteresis membranes. Int. J. Non. Linear. Mech. **147**, 104231 (2022). https://doi.org/10.1016/j.ijnonlinmec.2022.104231

Firouzi, N., Žur, K.K.: On the generalised nonlinear mechanics of compressible, incompressible, isotropic, and anisotropic hyperelastic membranes. Int. J. Solids Struct. **264**, 112088 (2023). https://doi.org/10.1016/j.ijsolstr.2022.112088

Gamage, T.P.B., Rajagopal, V., Ehrgott, M., Nash, M.P., Nielsen, P.M.F.: Identification of mechanical properties of heterogeneous soft bodies using gravity loading. Int. J. Numer. Method. Biomed. Eng. **27**(3), 391–407 (2011). https://doi.org/10.1002/CNM.1429

HajiRassouliha, A.: A toolbox for precise and robust deformation measurement [Doctoral thesis, The University of Auckland]. The University of Auckland Research Space (2017). https://researchspace.auckland.ac.nz/handle/2292/35955

HajiRassouliha, A., Babarenda Gamage, T.P., Parker, M.D., Nash, M.P., Taberner, A.J., & Nielsen, P.M.F.: 3D surface profiling using arbitrarily positioned cameras.

In: 2013 28th International Conference on Image and Vision Computing New Zealand (IVCNZ 2013) (2013)
HajiRassouliha, A., Taberner, A.J., Nash, M.P., Nielsen, P.M.F.: Subpixel phase-based image registration using Savitzky-Golay differentiators in gradient-correlation. Comput. vis. Image Underst. **170**, 28–39 (2018). https://doi.org/10.1016/j.cviu.2017.11.003
Han, S.P.: A globally convergent method for nonlinear programming. J. Optim. Theory Appl. **22**(3), 297–309 (1977). https://doi.org/10.1007/BF00932858
He, H., Zhang, Q., Zhang, Y., Chen, J., Zhang, L., Li, F.: A comparative study of 85 hyperelastic constitutive models for both unfilled rubber and highly filled rubber nanocomposite material. Nano Mater. Sci. (2021). https://doi.org/10.1016/J.NANOMS.2021.07.003
Ho, L.V., Trinh, T.T., De Roeck, G., Bui-Tien, T., Nguyen-Ngoc, L., Abdel Wahab, M.: An efficient stochastic-based coupled model for damage identification in plate structures. Eng. Fail. Anal. **131**, 105866 (2022). https://doi.org/10.1016/j.engfailanal.2021.105866
Kim, B., et al.: A comparison among Neo-Hookean model, Mooney-Rivlin model, and Ogden model for Chloroprene rubber. Int. J. Precis. Eng. Manuf. **13**(5), 759–764 (2012). https://doi.org/10.1007/s12541-012-0099-y
Kim, S., Jung, C.L., Jung, Y., Moon, H., Lim, H.: Biomimetic skin-type shear sensor. Int. Conf. Control. Autom. Syst. (2016). https://doi.org/10.1109/ICCAS.2016.7832484
Külcü, I.D.: A hyperelastic constitutive model for rubber-like materials. Arch. Appl. Mech. **90**(3), 615–622 (2019). https://doi.org/10.1007/S00419-019-01629-7
Lee, C., et al.: Soft robot review. Int. J. Control. Autom. Syst. **15**(1), 3–15 (2017). https://doi.org/10.1007/s12555-016-0462-3
Madireddy, S., Sista, B., Vemaganti, K.: A Bayesian approach to selecting hyperelastic constitutive models of soft tissue. Comput. Methods Appl. Mech. Eng. **291**, 102–122 (2015). https://doi.org/10.1016/J.CMA.2015.03.012
Makinde, A., Thibodeau, L., Neale, K.W.: Development of an apparatus for biaxial testing using cruciform specimens. Exp. Mech. **32**(2), 138–144 (1992). https://doi.org/10.1007/BF02324725
Martins, P.A.L.S., Jorge, R.M.N., Ferreira, A.J.M.: A comparative study of several material models for prediction of hyperelastic properties: application to silicone-rubber and soft tissues. Strain **42**(3), 135–147 (2006). https://doi.org/10.1111/j.1475-1305.2006.00257.x
Martins, P.A.L.S., Natal Jorge, R.M., Ferreira, A.J.M.: A comparative study of several material models for prediction of hyperelastic properties: application to silicone-rubber and soft tissues. Strain **42**(3), 135–147 (2006). https://doi.org/10.1111/j.1475-1305.2006.00257.x
Minh, H.-L., Sang-To, T., Khatir, S., Abdel Wahab, M., Cuong-Le, T.: Damage identification in high-rise concrete structures using a bio-inspired meta-heuristic optimisation algorithm. Adv. Eng. Softw. **176**, 103399 (2023). https://doi.org/10.1016/j.advengsoft.2022.103399
Nasab, A.M., Sabzehzar, A., Tatari, M., Majidi, C., Shan, W.: A soft gripper with rigidity tunable elastomer strips as ligaments. Soft Robot. **4**(4), 411–420 (2017). https://doi.org/10.1089/SORO.2016.0039/ASSET/IMAGES/LARGE/FIGURE8.JPEG
Nathanson, M.H., Saidel, G.M.: Multiple-objective criteria for optimal experimental design: application to ferrokinetics. Am. J. Physiol. **248**(3), R378–R386 (1985). https://doi.org/10.1152/AJPREGU.1985.248.3.R378
Nguyen, B.H., Zhuang, X., Wriggers, P., Rabczuk, T., Mear, M.E., Tran, H.D.: Isogeometric symmetric Galerkin boundary element method for three-dimensional elasticity problems. Comput. Methods Appl. Mech. Eng. **323**, 132–150 (2017). https://doi.org/10.1016/j.cma.2017.05.011
Nguyen-Thanh, V.M., Anitescu, C., Alajlan, N., Rabczuk, T., Zhuang, X.: Parametric deep energy approach for elasticity accounting for strain gradient effects. Comput. Methods Appl. Mech. Eng. **386**, 114096 (2021). https://doi.org/10.1016/j.cma.2021.114096
Nguyen-Thanh, N., Nguyen-Xuan, H., Bordas, S.P.A., Rabczuk, T.: Isogeometric analysis using polynomial splines over hierarchical T-meshes for two-dimensional elastic solids. Comput. Methods Appl. Mech. Eng. **200**(21–22), 1892–1908 (2011). https://doi.org/10.1016/j.cma.2011.01.018
Nguyen-Thanh, V.M., Zhuang, X., Rabczuk, T.: A deep energy method for finite deformation hyperelasticity. Eur. J. Mech. A Solids **80**, 103874 (2020). https://doi.org/10.1016/j.euromechsol.2019.103874
Payne, T., Mitchell, S., Bibb, R., Waters, M.: The evaluation of new multi-material human soft tissue simulants for sports impact surrogates. J. Mech. Behav. Biomed. Mater. **41**, 336–356 (2015). https://doi.org/10.1016/j.jmbbm.2014.09.018
Ranzani, T., Gerboni, G., Cianchetti, M., Menciassi, A.: A bioinspired soft manipulator for minimally invasive surgery. Bioinspir. Biomim. **10**(3), 035008 (2015). https://doi.org/10.1088/1748-3190/10/3/035008
Rao, M.R., Satayanarayana, P.M.R.S.: On the behaviour of hyperelastic materials, a Mooney-Riviln approach. Int. J. Eng. Res. Technol. **7**(3) (2019) Accessed from 04 Oct 2021. [Online]. Available: www.ijert.org
Roberts, P., Damian, D. D., Shan, W., Lu, T., Majidi, C.: Soft-matter capacitive sensor for measuring shear and pressure deformation. In: Proc. - IEEE Int. Conf. Robot. Autom., pp. 3529–3534, (2013). https://doi.org/10.1109/ICRA.2013.6631071
Sang-To, T., Hoang-Le, M., Wahab, M.A., Cuong-Le, T.: An efficient planet optimization algorithm for solving engineering problems. Sci. Rep. **12**(1), 8362 (2022). https://doi.org/10.1038/s41598-022-12030-w
Sang-To, T., Le-Minh, H., Abdel Wahab, M., Thanh, C.-L.: A new metaheuristic algorithm: Shrimp and Goby association search algorithm and its application for damage identification in large-scale and complex structures. Adv. Eng. Softw. **176**, 103363 (2023). https://doi.org/10.1016/j.advengsoft.2022.103363
Sareh, S et al.: Bio-inspired tactile sensor sleeve for surgical soft manipulators. In: Proceedings - IEEE international conference on robotics and automation, pp. 1454–1459, (2014). https://doi.org/10.1109/ICRA.2014.6907043
Sarkar, D., Dasgupta, S., Reddy, S.N., Arora, A., Sen, S.: A soft bending-type actuator using hyper-elastic materials: development, analysis and characterisation. In: ACM International Conference Proceeding Series, pp. 1–7, (2019). https://doi.org/10.1145/3352593.3352668

Sasso, M., Palmieri, G., Chiappini, G., Amodio, D.: Characterisation of hyperelastic rubber-like materials by biaxial and uniaxial stretching tests based on optical methods. Polym. Test. **27**(8), 995–1004 (2008). https://doi.org/10.1016/J.POLYMERTESTING.2008.09.001

Schittkowski, K.: NLQPL: a FORTRAN-subroutine solving constrained nonlinear programming problems. Ann. Oper. Res. **5**, 485–500 (1985)

Shahzad, M., Kamran, A., Siddiqui, M.Z., Farhan, M.: Mechanical characterisation and FE modelling of a hyperelastic material. Mater. Res. **18**(5), 918–924 (2015). https://doi.org/10.1590/1516-1439.320414

Shivapooja, P., et al.: Dynamic surface deformation of silicone elastomers for management of marine biofouling: laboratory and field studies using pneumatic actuation. Biofouling **31**(3), 265–274 (2015). https://doi.org/10.1080/08927014.2015.1035651

Smooth-On (n.d.) Ecoflex 00-50. Retrieved from https://www.smooth-on.com/products/ecoflex-00-50/

Sorooshian, S., Arfi, F., Sorooshian, S., Arfi, F.: Response Surface parameter sensitivity analysis methods for postcalibration studies. WRR **18**(5), 1531–1538 (1982). https://doi.org/10.1029/WR018I005P01531

Sparks, J.L., et al.: Use of silicone materials to simulate tissue biomechanics as related to deep tissue injury. Adv. Ski. Wound Care **28**(2), 59–68 (2015). https://doi.org/10.1097/01.ASW.0000460127.47415.6e

Standard Test Methods for Vulcanized Rubber and Thermoplastic Elastomers—Tension. https://www.astm.org/d0412-16r21.html Accessed from 07 Jun 2022

Steinmann, P., Hossain, M., Possart, G.: Hyperelastic models for rubber-like materials: consistent tangent operators and suitability for Treloar's data. Arch. Appl. Mech. **82**(9), 1183–1217 (2012). https://doi.org/10.1007/S00419-012-0610-Z

Tobajas, R., Ibartz, E., Gracia, L.: A comparative study of hyperelastic constitutive models to characterize the behavior of a polymer used in automotive engines. In: Proceedings of the 2nd International Electronic Conference on Materials, MDPI, Basel, Switzerland (2016). https://doi.org/10.3390/ecm-2-A002

Tran, V.-T., Nguyen, T.-K., Nguyen-Xuan, H., Abdel Wahab, M.: Vibration and buckling optimisation of functionally graded porous microplates using BCMO-ANN algorithm. Thin-Walled Struct. **182**, 110267 (2023). https://doi.org/10.1016/j.tws.2022.110267

Ultimaker 2+ 3D printer. https://ultimaker.com/3d-printers/ultimaker-2-plus-connect Accessed from 10 Feb 2022

Voyiadjis, G.Z., Oucif, C., Kattan, P.I., Rabczuk, T.: Damage and healing mechanics in plane stress, plane strain, and isotropic elasticity. Int. J. Damage Mech. **29**(8), 1246–1270 (2020). https://doi.org/10.1177/1056789520905347

Yap, H.K., Lim, J.H., Nasrallah, F., Cho Hong Goh, J., Yeow, C.-H.: Characterisation and evaluation of soft elastomeric actuators for hand assistive and rehabilitation applications. J. Med. Eng. Technol. **40**(4), 199–209 (2016). https://doi.org/10.3109/03091902.2016.1161853

Zhang, X., et al.: Adjustable compliance soft sensor via an elastically inflatable fluidic dome. Sensors **21**, 1970 (2021). https://doi.org/10.3390/S21061970

Zhao, Z., Mu, X., Du, F.: Modeling and verification of a new Hyperelastic model for rubber-like materials. Math. Probl. Eng. (2019). https://doi.org/10.1155/2019/2832059